Journal Pre-proof

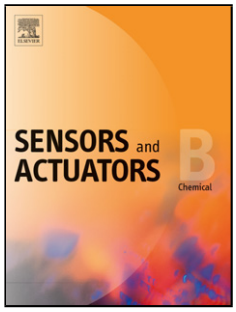

Synthesis, characterization, DFT study, conductivity and effects of humidity on CO_2 sensing properties of the novel tetrakis-[2-(dibenzylamino)ethoxyl] substituted metallophthalocyanines

Sema Şenoğlu, Metin Özer, Fatih Dumludağ, Nursel Acar, Bekir Salih, Özer Bekaroğlu

PII: S0925-4005(20)30207-0

DOI: https://doi.org/10.1016/j.snb.2020.127860

Reference: SNB 127860

To appear in: *Sensors and Actuators: B. Chemical*

Received Date: 28 August 2019

Revised Date: 8 January 2020

Accepted Date: 10 February 2020

Please cite this article as: Şenoğlu S, Özer M, Dumludağ F, Acar N, Salih B, Bekaroğlu Ö, Synthesis, characterization, DFT study, conductivity and effects of humidity on CO_2 sensing properties of the novel tetrakis-[2-(dibenzylamino)ethoxyl] substituted metallophthalocyanines, *Sensors and Actuators: B. Chemical* (2020), doi: https://doi.org/10.1016/j.snb.2020.127860

Synthesis, characterization, DFT study, conductivity and effects of humidity on CO_2 sensing properties of the novel tetrakis-[2-(dibenzylamino)ethoxyl] substituted metallophthalocyanines

Sema Şenoğlu[a], Metin Özer*[a], Fatih Dumludağ[b], Nursel Acar*[c], Bekir Salih[d], Özer Bekaroğlu*[e]

[a]*Department of Chemistry, Marmara University, 34722 Göztepe Istanbul, Turkey senoglusema@hotmail.com*

**metinozer@marmara.edu.tr*

[b]*Department of Physics, Marmara University, 34722 Göztepe Istanbul, Turkey fatihdumludag@marmara.edu.tr*

[c]*Department of Chemistry, Ege University, 35100 Bornova İzmir, Turkey *nursel.acar@ege.edu.tr*

[d]*Chemistry Department, Hacettepe University, 06800 Beytepe Ankara, TURKEY bekir@hacettepe.edu.tr*

[e]*Faculty of Pharmacy, Istinye University, 34010, Zeytinburnu Istanbul, Turkey *obek@itu.edu.tr*

Corresponding authors:

E-mail: metinozer@marmara.edu.tr (Metin Özer);

E-mail: nursel.acar@ege.edu.tr (Nursel Acar);

Department of Chemistry, Faculty of Science,

Ege University, Bornova, Izmir, TR-35100, TURKEY

Tel: + 90 232 3112382

Fax: +90 232 3888264

ORCID ID: 0000-0001-9292-0637

E-mail: obek@itu.edu.tr (Özer Bekaroğlu)

Graphical abstract

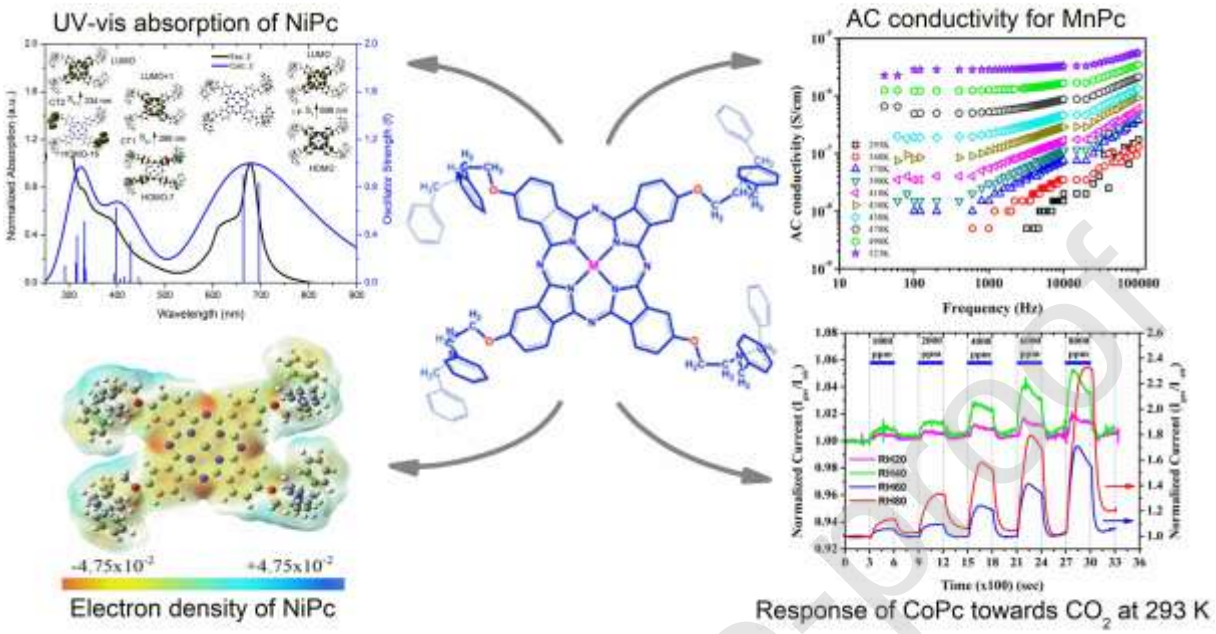

Calculated electrostatic potentials, calculated and experimental UV-Vis spectra of the investigated metallophthalocyanines accompanied by the results for DC conductivity ($\sigma_{(MnPc)}<\sigma_{(NiPc)}<\sigma_{(CoPc)}$), CO_2 sensing properties, and effect of humidity on CO_2 sensing properties were reported.

Highlights

- New CO_2 sensing metallophthalocyanines were synthesized and characterized.
- Experimental and computational techniques were used for characterization.
- Gas concentration and humidity effects on CO_2 sensing of the phthalocyanines were determined at 293 K.
- Mn phthalocyanine showed greater sensitivity than Ni- and Co phthalocyanines.

ABSTRACT

Novel tetrakis-[2-(dibenzylamino)ethoxyl] substituted nickel (II), cobalt (II) and manganese (II) phthalocyanines were synthesized by using 4-(2-(dibenzylamino)ethoxy)phthalonitrile with corresponding metal salts in 2-N, N-dimethylaminoethanol. New phthalonitrile ligand was prepared from 2-(dibenzylamino)ethan-1-ol and 4-nitrophthalonitrile in acetonitrile at reflux temperature using potassium carbonate as catalyst. The compounds was characterized by elemental analysis, infrared, ultraviolet–visible and matrix-assisted laser desorption/ionization time-of-flight mass spectroscopic methods. Density functional theory calculations were performed for structural and electronic properties. Direct current and alternating current conductivity properties of the metallophthalocyanine films were investigated between 293-523 K and frequencies 40-100 kHz. The direct current conductivity values were calculated as $5.29x10^{-10}$ S/cm, $2.39x10^{-9}$ S/cm, and $3.04x10^{-10}$ S/cm, for nickel, cobalt and manganese complexes (293 K) films, respectively. Activation energies of the films were 0.50-0.70 eV for T< 478 K. Alternating current conductivity results suggest that hopping model explains dominant charge transport mechanisms. Carbon dioxide sensing properties (1000- 8000 ppm) of the metallophthalocyanine films were investigated at room temperature (293 K) in air as background. Additionally, effects of the relative humidity on carbon dioxide sensing properties were also investigated for relative humidity between 0-80% RH in air. Response and response time values of the films were reported. Newly synthesized phthalocyanine complexes in this study were found to be reversible and sensitive to the carbon dioxide gas in humid air. Carbon dioxide sensing measurements revealed that sensitivity of the sensors increased with increasing carbon dioxide concentration and relative humidity. It is found that manganese phthalocyanine showed greater sensitivity than nickel- and cobalt phthalocyanine complexes.

***Keywords**:* Phthalocyanine; MALDI-TOF MS; Density Functional Theory; Semiconductor; Conductivity; CO_2 sensing

1. Introduction

The Phthalocyanines (Pcs) are planar macrocyclic compounds having nitrogen in the nucleus cycle. Both substituents and metal ions have significant effects on the physical and chemical properties of phthalocyanines [1].

Owing to these modifiable features, their 18 π electronic structure, optical and high thermal properties; Pcs behave as efficient compounds in main scientific applications such as semiconductors and liquid crystals as sensors, molecular electronics, electrochromic systems, dye-based solar cells, nonlinear optical materials, cancer therapy and other medical applications as photodynamic materials [2,3]. Physical properties of phthalocyanines can be improved with the coordination of metal ions and the introduction of substituents at the peripheral or nonperipheral positions. It is possible to obtain unlimited number of new Pcs if several different metal ions are coordinated to the center of the Pc and a large number of different substituents are considered [4]. Thus, the structure of phthalocyanines can be tailored according to the targeted application mentioned above.

Potential applications of the materials depend on electrical properties such as conductivity. In order to clarify direct current (DC) and alternating current (AC) conductivity, charge transport mechanisms of the compounds and their electrical measurements were performed on the nickel (**2**)-, cobalt (**3**)- and manganese (**4**) phthalocyanine complexes between the temperatures of 293-523 K and frequency of 40-100 kHz.

Carbon dioxide (CO_2) is odorless and colorless gas and one of responsible gas for global warming due to its greenhouse effect. CO_2 can also cause health problems such as dizziness, headache, elevated blood pressure, increased heart rate, suffocation, and unconsciousness. In case of long-term or repeated exposure, CO_2 may have effects on the metabolism [5]. It has been reported that 100000 ppm (parts per million) is the atmospheric concentration immediately dangerous to life and that exposure to 100000 ppm for only a few minutes can cause loss of consciousness [6,7]. Permissible Exposure Limits (PEL) were declared as 5000

ppm as an 8 hour time weighted average (TWA) concentration and 30 000 ppm as a short term exposure limit (STEL, 15-minute TWA exposure that should not be exceeding at any time during a workday) for CO_2 by Occupational Safety Health and Administration (OSHA) [7] and REL and STEL by The National Institute for Occupational Safety and Health (NIOSH)-Centers for Disease Control and Prevention, respectively [7]. Hence the sensing of CO_2 is extremely important and there has been lots of efforts to investigate CO_2 sensing properties of potential sensing materials [8,9]. Since detection of CO_2 in air and also in humid air are more important than that of in another atmosphere such as nitrogen (N_2), effects of humidity on CO_2 sensing properties of the materials such as inorganic and organic materials were investigated before but most of them needs higher temperatures such as T> 160 ^oC [10].

Motivated by the gas sensing properties of metallophthalocyanines, a novel 4-(2-(dibenzylamino)ethoxyl) substituted metallophthalocyanines with redox active metal center have been synthesized and characterized with elemental analysis, FTIR, 1H-NMR and MALDI TOF mass spectroscopy methods. Additionally, proposed geometries of the compounds were confirmed by computational methods.

The effects of humidity (0-80% RH) on carbon dioxide sensing properties of the films complexes **2-4** were investigated at room temperature (293 K) in air. Several types of CO_2 sensors, working with different sensing mechanism, such as optical [11], surface acoustic wave (SAW) device [12], and conductometric sensors [9], have been reported but conductometric sensors have some advantages such as cheap, and mobile.

2. Experimental

2.1. Materials and methods

Electronic and IR spectra were acquired on a Shimadzu UV-2600 UV-VIS and a Shimadzu FTIR-8300 (ATR and KBr pellet) Spectrophotometers respectively. Elemental

analyses were achieved using the CHNS-932 (LECO). Mass spectra were performed on a Rapiflex MALDI-TOF-MS (Bruker Daltonics, Bremen-GERMANY) equipped with a Smartbeam 3D 10kHz 355 nm Nd: YAG laser applying 1000 laser shots per each sample spot using a single shot laser configuration. All MALDI-TOF-MS data were obtained at positive ion and reflectron mode. Calibration was accomplished with a series of peptides existing in a mixture (Bruker Daltonics standard) before mass spectrometric analysis of the samples. ^{1}H-NMR spectra of compounds were obtained on a Bruker Avance III 500 MHz, 1.74 Tesla spectrophotometer using TMS as internal standard.

2.2. MALDI TOF MS measurements

2.2.1 Sample preparation

For the samples, 2,5-dihydroxybenzoic acid as MALDI matrix, was prepared in H_2O-ACN-THF(10:45:45, v/v/v) containing 0.1% trifluoroacetic acid at a concentration of 10 mg/mL. Sample solutions (2 mg/mL in ACN-THF-DMFA (48:48:4, v/v/v) were prepared using 2 mg/mL in ACN-THF-DMFA (50:50:2, v/v/v). Finally 0.5 µL of MALDI matrix was deposited onto the MALDI plate after dried at room temperature 0.2 µL sample solution was deposited onto the same spot as an on spot preparation technique and then analyzed in MALDI-MS.

2.2.2. Preparation of films for electrical measurements

Electrical measurements were done using Interdigital Transducer (IDT) containing 10 pair of chromium/gold electrodes with width and space between the electrodes is 100 µm fabricated in our laboratory onto glass substrate. The solutions of the compounds were prepared in THF (Tetrahydrofuran, C_4H_8O), purchased from Merck, homogeneously at a concentration of $5x10^{-2}$ M at temperature of 293 K in nitrogen ambient. To prepare seemingly identical films, 50 µl of $5x10^{-2}$ M solutions of the compounds were dropped onto the gold electrodes by using micro-syringes at 293 K. Thin films of the compounds were obtained by

evaporating the solvent of the solution at 323 K in nitrogen atmosphere. The repeatability of the fabricated films was tested by examining dc and ac conductivity values at different temperatures and response towards the carbon dioxide (CO_2) gas at room temperature. The change in the values was calculated as nearly ~5% between the films.

2.2.3. Electrical measurements

Conductivity measurements were performed on the films of **2-4** between the temperatures 293-523 K and in the frequency range 0.04-100 kHz and in vacuum ($2x10^{-3}$ mbar), in dark. Temperature of the substrate of the films was controlled by a chromel-alumel thermocouple and a temperature controller. Current-Voltage (I-V) measurements were performed by applying dc voltages between -1 to 1 V to the electrodes of the IDT and recording the current values. DC and AC conductivity measurements were done by using Keithley model 6417B programmable electrometer and Keithley model 3330 LCZ meter, respectively. Before starting the electrical measurements the current values of the films were allowed to reach stable state at each measurement temperatures. All the data were recorded by personal computer using an IEEE-488 data acquisition system.

2.2.4. CO_2 Sensing Measurements

CO_2 sensing measurements of the sensors were done as a function of CO_2 concentration (1000-8000 ppm) at different relative humidity (0 - 80% RH) ambient in air (purity >99%) at room temperature. In order to prevent interactions between surface of the measurement chamber and humidity/CO_2 gas, sensing measurements were performed in teflon measurement chamber, instead of metal chamber. The CO_2 gas concentrations took placed between 1000-8000 ppm. All sensing measurements were performed by using computer controlled mass flow controllers (MKS Inst). Gas sensing properties were obtained for 300 seconds intervals; 300 seconds for CO_2 and 300 seconds for purging with air (0-80% RH). During the gas sensing measurements, dc voltage of 1 V was applied to the electrodes of the

IDTs. Gas sensing measurements were performed after the current passing through the sensor in air is constant (steady-state). Gas sensing measurement system was equipped by IEEE-488 data acquisition system. Response of the sensors was examined by means of change in dc conductivity of the sensors as a function of gas concentration at different relative humidities (RH).

2.3. Synthesis

2.3.1. Synthesis of phthalonitrile compound (1) (Scheme 1)

A mixture of 3.86 g (0.016 mol) 2-(dibenzylamino)ethan-1-ol, 2.77 g (0.016 mol) 4-nitrophthalonitrile and (6.62 g (0.048 mol) K_2CO_3 was refluxedin acetonitrile (40 ml) with magnetic stirring in 100 ml of a round bottomed flask for 24 h. The cooled reaction mixture was poured into iced water (150 ml) with stirring. The creamy precipitate was filtered off and washed with water until the filtrate was neutral, and dried in room temperature. The product with impurities was separated by column chromatography with silica gel using chloroform as eluent. This compound **1** is easily soluble in common organic solvents such as THF, MeOH, EtOH, $CHCl_3$, CH_2Cl_2 and acetone. Yield: 4.36 g (75%). Mp 182 °C. Anal. Calcd. for $C_{24}H_{21}N_3O$: C, 78.45; H, 5.76; N, 11.44%. Found: C, 77.23; H, 5.73; N, 11.47 %; IR (ATR) $\bar{\upsilon}/cm^{-1}$: 3068 (Arom CH), 2941-2920 (Aliph CH), 2232 (C≡N), 1602-1410 (C=C), 1230 (C-O-C). ^{1}H-NMR δ, ($CDCl_3$): 2.96 (t, 2H, -CH_2 aliph-H_1), 3.77 (s, 4H, -CH_3 aliph-H_2), 4.07 (t, 2H, -CH_2 aliph-H_3), 7.06 (d, 1H, Ar-H_4), 7.15 (s, 1H, Ar-H_5), 7.33 (t, 2H, Ar-H_6), 7.38 (t, 4H, Ar-H_7), 7.43 (d, 4H, Ar-H_8), 7.68 (d, 1H, Ar-H_9) (Scheme 1, Fig. 1-4).

2.3.2. 2(3), 9(10), 16(17), 23(24) -4-(2-(dibenzylamino)ethoxy) phthalocyanine nickel (II) complex (2). (Scheme 1)

A mixture of 0.22g (0.58 mmol) 4-(2-(dibenzylamino) ethoxy) phthalonitrile (1), 0.036 g (0.14 mmol) $Ni(CH_3COO)_2$.4H2O and 2 ml of 2-(N,N-dimetilamino)etanol (DMA) was heated in a vacuum-packed glass tube for 4 hours under a dry N_2 atmosphere at 300 °C. The

reaction mixture was precipitated after cooling to room temperature by pouring in to the cold water and then washed with acetone. Following filtration of the precipitate, it was washed with hot water, methanol and acetone in the soxhalet apparatus for 24 hours respectively.

The purification of the crude product was performed by dissolving it in about 3 ml of DMF and then reprecipitating by the addition of acetone. NiPc **2** is soluble in THF, DMF and DMSO. Mp > 300°C. Yield: 0.096 g (43%), Anal. Calcd. for $C_{96}H_{84}N_{12}NiO_4$: C, 75.44; H, 5.54; N, 11.00%. Found: C, 74.83; H, 5.56; N, 11.07%. IR (ATR) $\bar{\upsilon}/cm^{-1}$: 3023 (arom C-H), 2938 (aliph C-H), 1602-1412 (C=C), 1346 (C-H bend), 1231 (C-O-C). UV-vis (DMF, $1.53x10^{-6}$ M) λ_{max} nm (log ε): 678 (5.69), 627 (4.91), 373 (5.30). MS (MALDI-TOF), m/z: 1527.61 $[M]^+$ (Scheme 1, Fig.5 and Fig.6(a)).

2.3.2. 2(3), 9(10), 16(17), 23(24) -4-(2-(dibenzylamino)ethoxy) phthalocyanine cobalt (II) complex (3). (Scheme 1)

A mixture of 0.20 g (0.56 mmol) 4-(2-(dibenzylamino) ethoxy) phthalonitrile (**1**),0.035 g (0.14 mmol) $Co(CH_3COO)_2.4H_2O$ and 2 ml of 2-(N,N-dimetilamino)etanol (DMA) was heated in a vacuum-packed glass tube under a dry N_2 atmosphere at 300 °C for 4 h. The isolation of **3** was succeeded by the same way used for **2**. The crude metallophthalocyanine **3** was purified by the same way as in the purification method of Ni (II) complex. CoPc **3** is soluble in THF, DMF and DMSO. Mp > 300 °C. Yield: 0.035 g (38%). Anal. Calcd. for $C_{96}H_{84}N_{12}CoO_4$: C, 75.43; H, 5.54; N, 10.99%. Found: C, 75.47; H, 5.44; N, 10.81%. IR (ATR) $\bar{\upsilon}/cm^{-1}$: 3020 (arom C-H), 2943 (aliph C-H), 1607-1407 (C=C), 1341 (C-H bend), 1211 (C-O-C). UV-vis (DMF, $2.31x10^{-6}$ M) λ_{max} nm (log ε): 673 (5.52), 613 (4.94), 332 (5.37). MS (MALDI-TOF), m/z: 1617.66 $[M]^+$, 1708.66 $[M+(CH_3)_2NCH_2OH+2H]^+$(Scheme 1, Fig.5 and Fig.6(b)).

2.3.2. 2(3), 9(10), 16(17), 23(24) -4-(2-(dibenzylamino)ethoxy) phthalocyanine manganese (II) complex (4). (Scheme 1)

A mixture of 0.076 g (0.21mmol) 4-(2-(dibenzylamino) ethoxy) phthalonitrile(**1**),0.013 g (0.052mol) $Mn(CH_3COO)_2.4H_2O$and 2 ml of 2-(N,N-dimetilamino)etanol (DMA) was heated in a closed and deaerated glass tube under a dry N_2 atmosphere at 300 °C for 4 h. The same purification method of complexes **2** and **3** were applied to complex **4**. MnPc **4** is soluble in THF, DMF and DMSO. Mp > 300°C. Yield: 0.023 g (29%). Anal. Calcd. for $C_{96}H_{84}N_{12}MnO_4$: C, 75.62; H, 5.55; N, 11.02%. Found: C, 75.58; H, 5.51; N, 11.05%. IR (ATR) $\bar{\upsilon}/cm^{-1}$: 3023 (Arom C-H), 2945 (Aliph C-H), 1603-1456 (C=C), 1338 (C-H bending), 1230 (C-O-C). UV-vis (DMF, $2.31x10^{-6}$ M) λ_{max} nm (log ε): 728 (3.79). MS (MALDI-TOF), m/z: 1523.62$[M]^+$(Scheme 1, Fig.5 and Fig.6(c)).

2.4. Computational details

Optimizations of studied molecules were carried out by Gaussian09 [13] and molecular structures were visualized by Gaussview 5.0 [14]. Geometry optimizations were carried out with Density Functional Theory (DFT) [15] at ground state. The hybrid B3LYP functional (B3: Becke's three-parameter nonlocal exchange functional [16,17] LYP: Lee-Yang-Parr's correlation function [18] was used with the 6-31G(d,p) basis set and with LANL2DZ basis set [19] (only for metals). True minimum natures of optimized structures were verified with all positive frequencies. The Polarizable Continuum Model (PCM) [20,21] was used with the inclusion of N,N-dimethylformamide (DMF) as solvent. The time-dependent DFT (TD-DFT) method was used to calculate the UV-Vis absorption spectra with B3LYP using the same basis set in order to compare with experimental UV-Vis absorption spectra. Vertical excitation calculations were performed using the first 100 singlet excited states for each system.

3. Results and discussion

3.1. Synthesis and characterization

The synthesis of starting material, 4-(2-(dibenzylamino) ethoxy) phthalonitrile (**1**) was justified by the loss of the NO_2 band at around 1350 cm^{-1} and the rise of a new absorption band at 1230 cm^{-1} for Ar–O–Ar bond in its IR spectrum. In addition, thetetramerization reaction of the nitrile derivative **1** leading to the formation of Pc complexes **2–4** was verified by the disappearance of the nitrile band around 2232 cm^{-1} in their IR spectra. On the other hand, the IR spectra of the Pcs gave the close wavenumber values like 3023 cm^{-1}, 3020 cm^{-1} and 3023 cm^{-1} (arom C-H), 2938 cm^{-1}, 2943 cm^{-1} and 2945 cm^{-1} (aliph C-H), 1602-1412 cm^{-1}, 1607-1407cm^{-1} and 1603-1456 cm^{-1} (C=C), 1231 cm^{-1}, 1211 cm^{-1} and 1230 cm^{-1} (C-O-C) for **2**, **3** and **4** respectively.

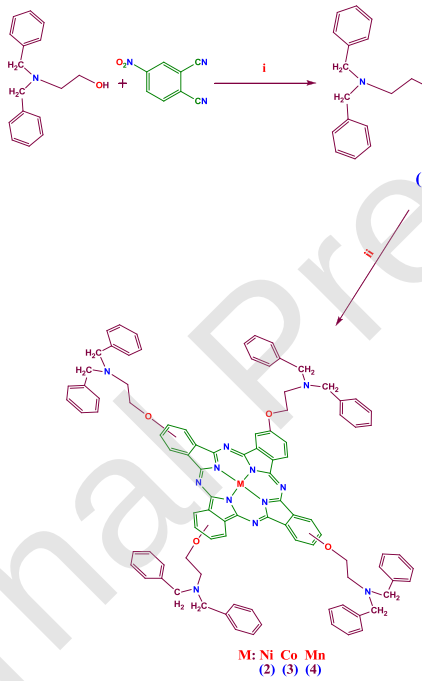

Scheme 1. i: K_2CO_3, DMF, 50 ^oC; ii: Metal(II) acetates, DMAE, 300 ^oC.

The ^{1}H-NMR spectrum of the starting material **1** (in C*D*Cl_3) showed satisfactory results for characterization about its suggested structure. H1, H2 and H3 indicate the aliphatic methylene (-CH_2-) protons at 2.96 ppm as triplet, 3.77 ppm as singlet and 4.06 ppm as triplet respectively (Fig.1).

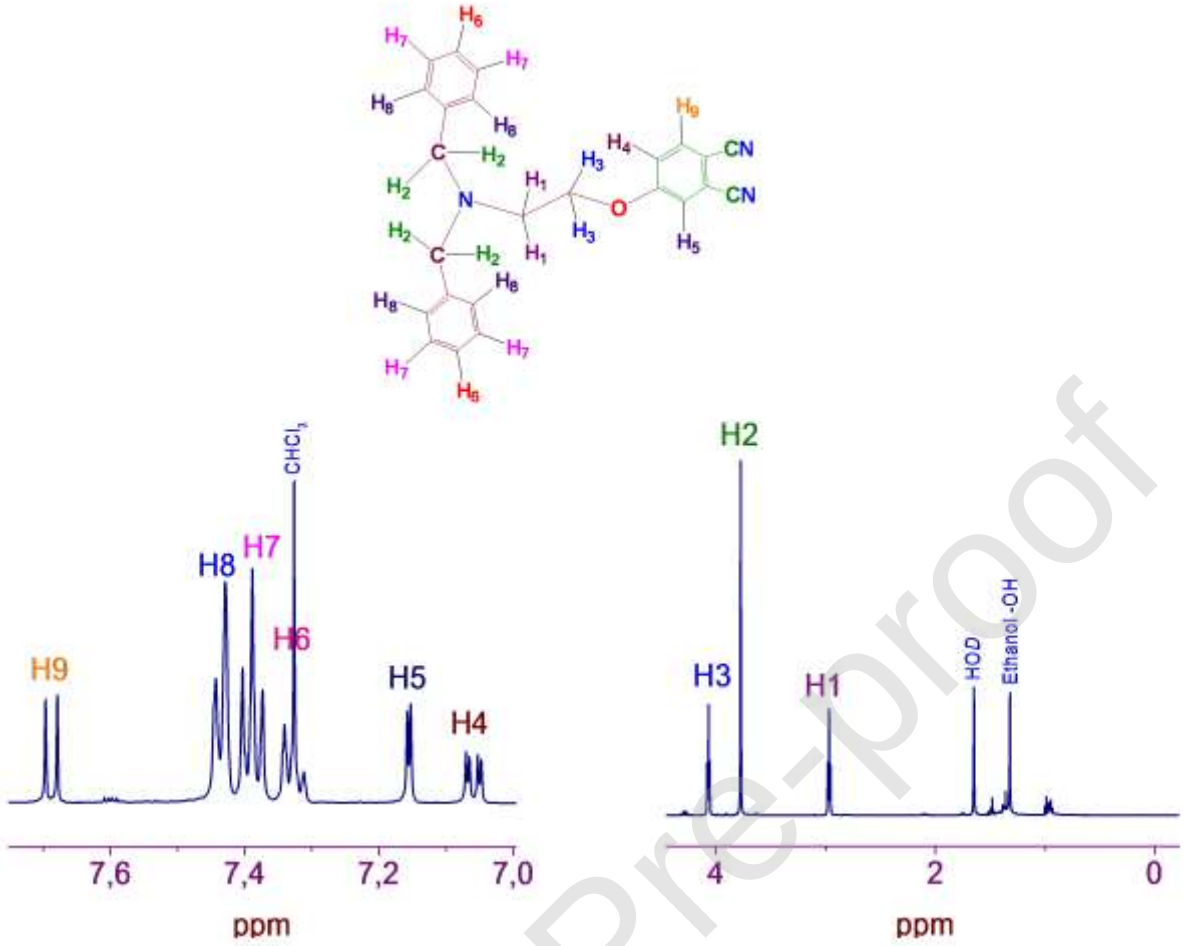

Fig. 1. The phthalonitrile compound 1 and its aromatic and aliphatic regions ^{1}H-NMR spectra.

As the aromatic region, H4, H8 and H9 gave the double doublet at 7.05 ppm, doublets at 7.43 and 7.68 ppm, respectively. Besides, H7 and H6 indicated triplets at 7.32 and 7.38 ppm in turn. In addition, a doublet band having a splitting of 2.56 Hz with meta-coupling was observed for H5 at 7.15 ppm. On the other hand, the aromatic region ^{1}H-NMR signals of NiPc complex (**2**) were broad. Thus, it was difficult to characterize it (Fig. 1).

The ^{1}H-^{1}H COSY spectrum of compound **1** showed that its synthesis and isolation was successfully achieved. The data on the H that are coupling with each other is obtained by looking at the peaks inside the 2D NMR.

The spot marked with A indicates a coupling interaction between the H1-H3 protons. This corresponds to the coupling of the adjacent methylene (-CH_2-CH_2-) protons on the alkane moiety. In the case of methylene protons H2 bonded with tertiary amine nitrogen atom, as they are in the same chemical environment there is no interaction between them, therefore the two H2 atoms gave the singlet peak at 3.77 ppm. Similarly, the spot marked B indicates a coupling interaction between H4 and H9. This corresponds to the matchup of the aromatic H4 at 7.05 ppm and the H9 at 7.68 ppm in the nitrile substituted benzene group (Fig.2).

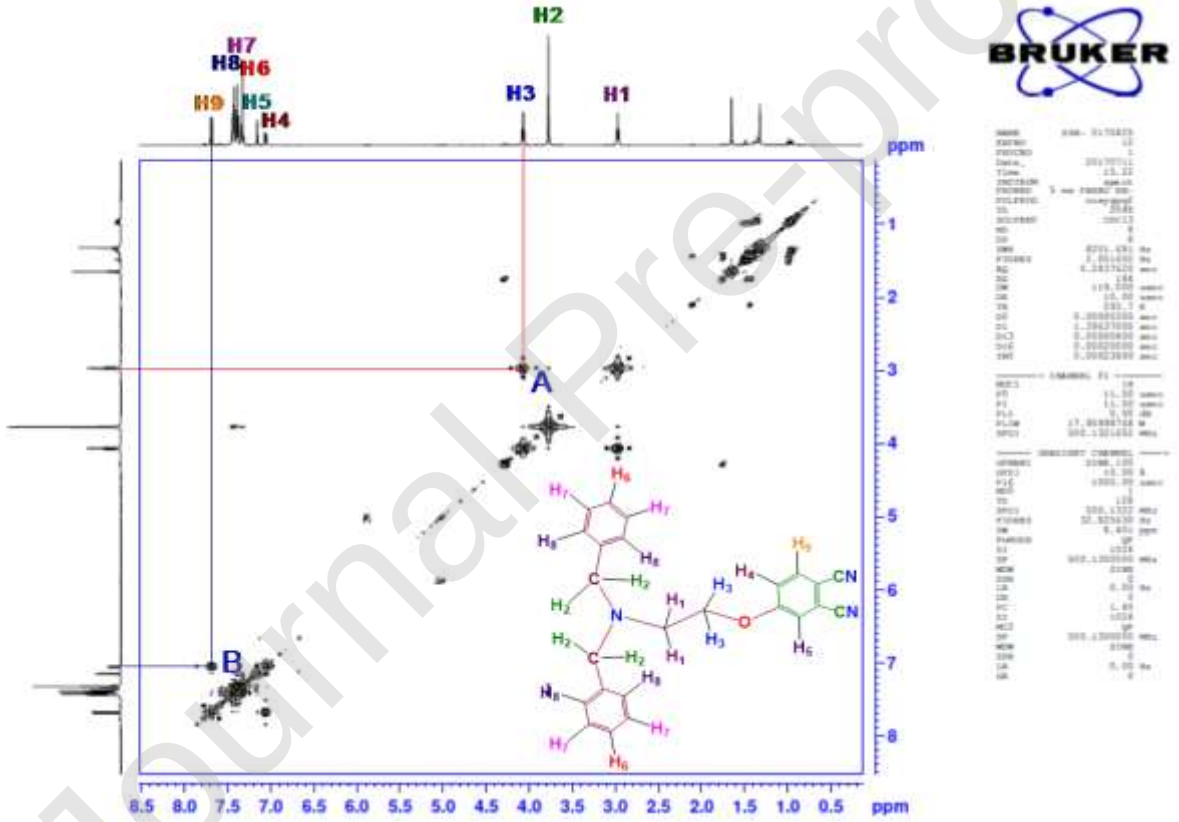

Fig. 2. The ^{1}H-^{1}H COSY-NMR spectrum of **1**.

In addition, UV-vis spectra of all complexes **2**, **3** and **4** showed typical absorptions in the Q band region at 678 nm 668 nm and 730 nm in DMF, respectively. Although complexes **2** and **3** demonstrated satellite bands at 622 nm and 607 nm in turn, that of

the manganese complex **4** gave the broad band between 605-690 nm. These metallophthalocyanines also showed Soret bands at about 385 nm 329 nm and 359 nm for **2**, **3** and **4** respectively (Fig.3).

In all samples 2, 5-dihydroxy benzoic acid was used as a MALDI matrix with the best signal intensity. The monoisotopic mass of each complexes showed that complexes were ionized in radical cationic form losing one electron not in protonated form in positive ion mode even if the samples consisting MALDI matrice and the sample acidified. This shows that radical cationic forms of the complexes are very stable under the laser firing in MALDI-MS conditions. On the other hand, in the case of cobalt complex **3** which is shown in Fig. 3, as well as radical cationic form of the complex, protonated ionization form is also available when the isotopic distribution of the molecular ion signals of complex either in theoretical or experimental forms which are given overlay spectrum inset.

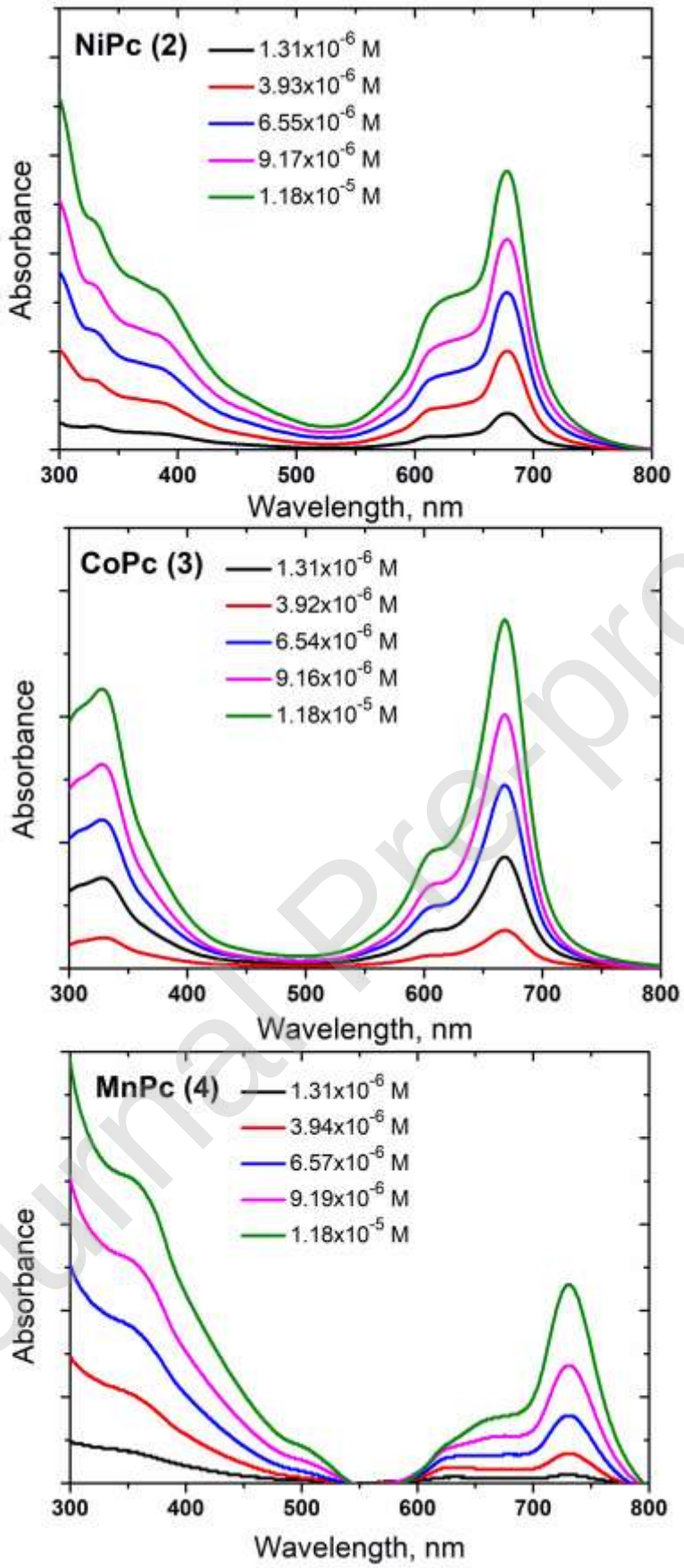

Fig. 3. UV-vis spectra of **2**, **3** and **4** in DMF

As seen from the inset spectrum when the intensities of the theoretical and experimental spectrum have the same intensity for the first peak (at the lowest mass), experimental signal intensities in the second and followed peaks were exceeded the signal intensities of the theoretical signal. This shows that both ionizations (in the radical cation and protonated cation forms) are possible under the MALDI-MS conditions but favorable ionization taken place in radical cation form when the intensities of the experimental and theoretical signals were compared.

The other critical observation is to about fragmentation or a fragment adducts to molecular ions of complexes which represented the benzyl group having 91 Da mass. This fragmentation was taken place on the side chain of the complexes due to the benzyl groups attached to the complexes via nitrogen atoms. The bond energy between carbon and nitrogen is the least compared to the other bond energies in the complexes. For this reason, this bond is weak and easily broken under the laser energy and fragmentation could be seen. On the other hand, CoPc **3**, indicated more two peaks due to the one and two 2-dimethylaminoethanol adducts having 89 Da mass in addition to molecular ion signal.

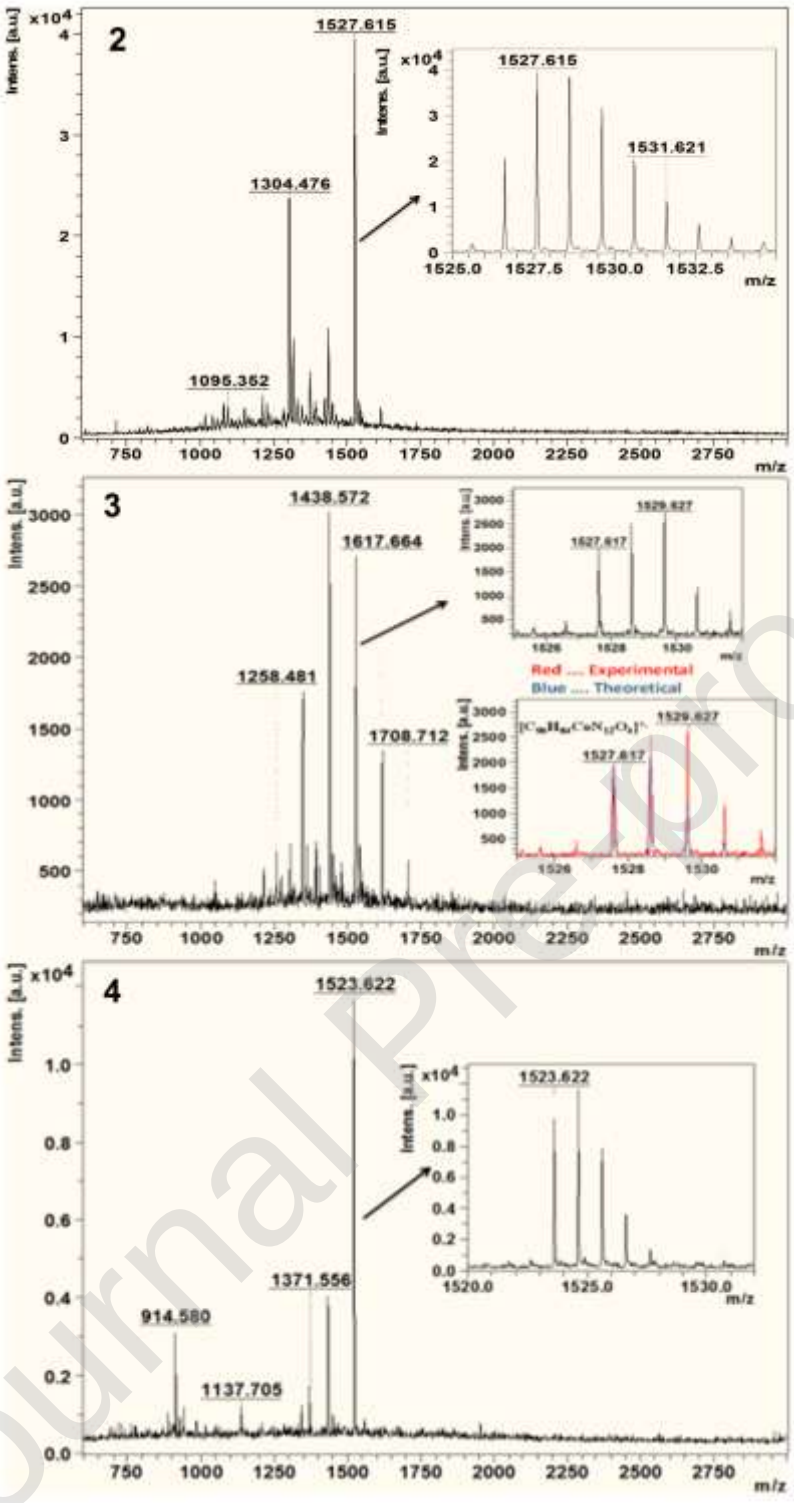

Fig. 4. Mass spectra of **2**, **3** and **4** acquired on a Rapiflex MALDI-TOF-MS (Bruker Daltonics, Bremen-GERMANY) equipped with a Smartbeam 3D 10 kHz 355 nm Nd: YAG laser applying 1000 laser shots per each sample spot using a single shot laser configuration.

3.2. Computational results

The optimized structures of the compoundsin ground-state are given in Fig. 5 in DMF at B3LYP/6-31G(d,p) level with LANL2DZ on metals. Because of the many single bonds in the molecules, the benzylamine group (ligand) was first optimized separately (Table S1). Conformer **C01** [22] was found to have the lowest energy and it was used in Pcs (Fig. S1).

Total electronic energies including zero point energy corrections (E_{elec}+ZPE, Hartree) and dipole moments (μ, Debye) of studied molecules are given in Table S2. Pcs have planar structures and dipole moments of the molecules are close to zero. Ligand N atom preserves its pyramidal structure.

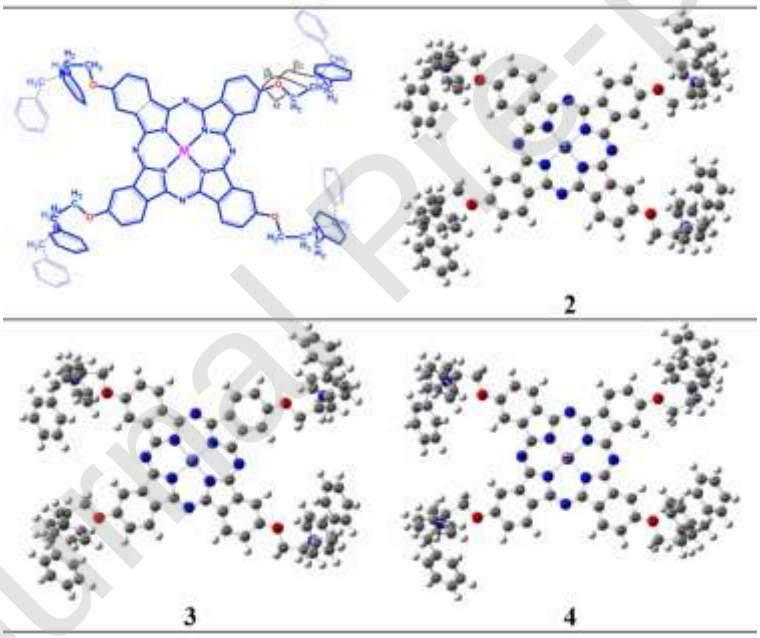

Fig. 5. Optimized geometries of compounds **2**, **3** and **4** in DMF calculated at B3LYP/6-31G(d,p) level (LANL2DZ used for metals)

TD-DFT calculations are performed (on the optimized ground-state geometries) to present molecular orbitals and to determine intramolecular ligand-metal charge

transfers. Those calculations are also used to calculate the UV-Vis absorption spectra (N=100 singlet states) and molecular orbital energies (E_{HOMO}, E_{LUMO}, E_{H-L}) in DMF. Because of the odd number of total electrons (Co(II) and Mn(II)), SOMOs (single occupied molecular orbitals) were shown with α-spin (Fig. S2). The energy difference between HOMO and LUMO was increased in the order of **2**<**3**<**4** in DMF. Having the smallest HOMO-LUMO gap, compound **2** is determined to be more suitable for the charge transfer applications.

Fig. 6 shows experimental and calculated UV-Vis absorption spectra and calculated oscillator strengths in DMF of compounds **2**, **3** and **4**. They also give information about the orbitals involved in the electronic transitions of molecules. The first transitions to Mn and Co have shifted to the IR region and are therefore not listed. Electronic transitions may be grouped into three: transitions including only Pcs (LE Pc: local excitation of Pc), transitions including ligands (phenyls) and Pcs (CT: intramolecular charge transfer), and transitions including metal and Pcs (MLCT: metal-to-ligand charge transfer or LMCT: ligand-to-metal charge transfer).

Q-band (LE Pc) was calculated as 696 nm, 686 nm and 661 nm between HOMO/SOMO and LUMO for **2**, **3** and **4** in DMF, respectively. Electronic transitions between Pc and ligands occurred in two ways: First, charge transitions from "N in benzylamine and O in Pc" to "Pc" core (CT1, n-π*), second, charge transitions from "benzyl groups" to "Pc core" (CT2, π-π*). Lists of electronic transitions and corresponding orbitals were given for **2**, **3** and **4**, in Table S3-S5 and Fig. S3-S5, respectively.

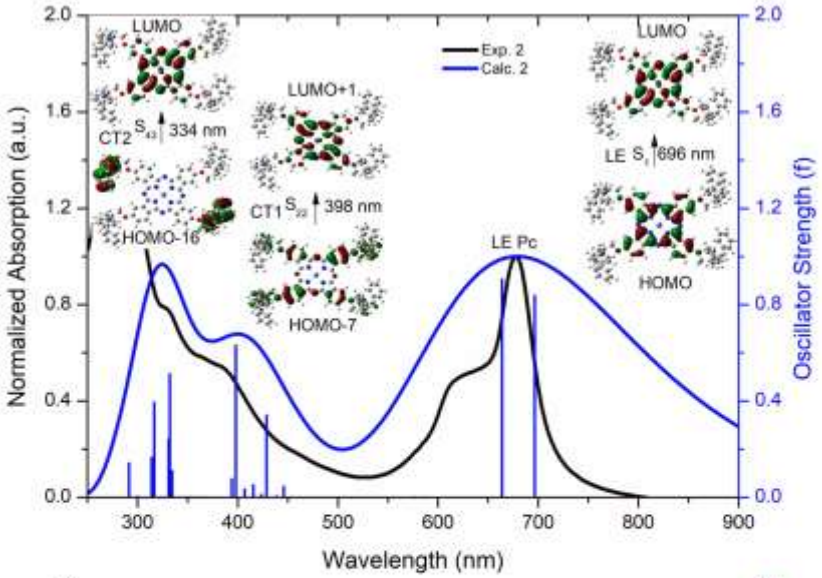

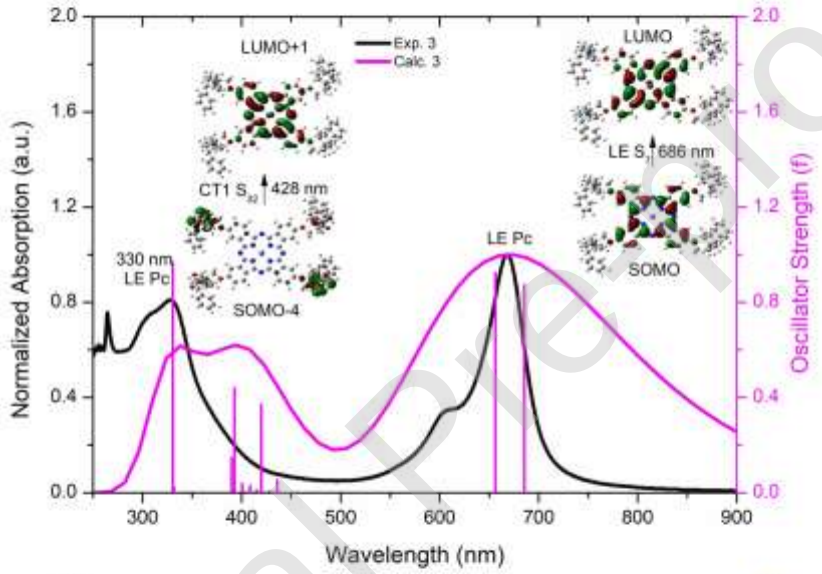

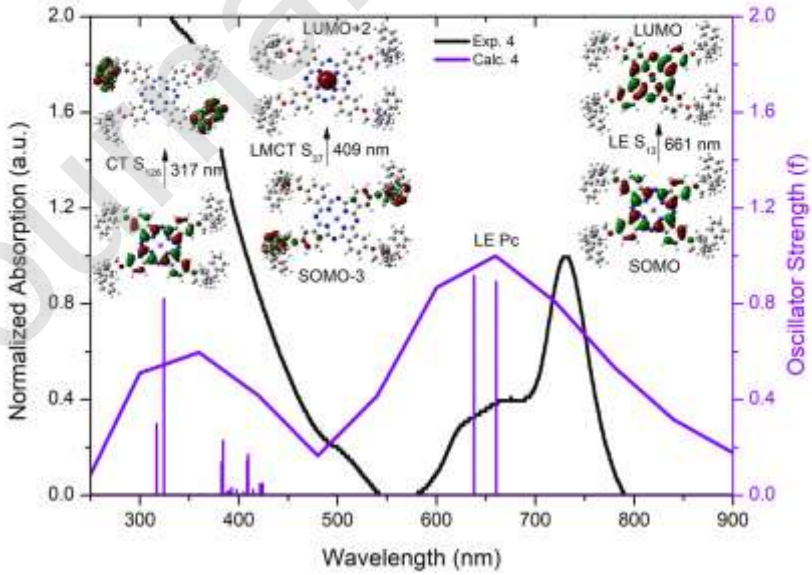

Fig. 6. Experimental (black line) and calculated (blue line: **2**, pink line: **3**, purple line: **4**) UV-Vis absorption spectra and calculated oscillator strengths for **2, 3** and **4** in DMF

At short wavelengths, charge transfer peaks between ligands and Pc are observed in addition to Soret bands. Electronic transitions of **2** (Table S3) have CT1 character between 366 nm and 577 nm, and display CT2 character between 323 nm and 361 nm. Soret band is calculated as 331 nm. Although Ligand-to-metal charge transfers from Pc to Ni (LMCT1) are calculated at 577 nm and 587 nm, their oscillator strengths are zero. On the other hand, there is a ligand-to-metal charge transfer from N and O to Ni (LMCT2) calculated at 337 nm with a low oscillator strength. Additionally, a metal-to-ligand charge transfer peak from Ni to Pc core which requires high energy (291 nm) is observed.

Q-bands at longer wavelength for compound **3** (656 nm and 686 nm) are followed by CT1 peaks between 390 nm and 507 nm (Table S4). CT1 peak at 420 nm has a high oscillator strength. There is a significant Soret band at 330 nm. CT2 peak occurs between 342 nm and 352 nm with a low oscillator strength. There are no MLCT observed in the investigated region.

Q-bands are calculated at 638 nm and 661 nm for electronic transitions of **4**. Soret band is observed at 324 nm. CT1 peak at 410 nm has a high oscillator strength (Table S5). LMCT2 (low oscillator strength) is observed at 409 nm de LMCT2 different than the other investigated systems. Additionally, the peak observed at 380 nm carries both LMCT2 and LMCT1 characters. Different from other systems, 150 singlet states were used to obtain electronic transitions at shorter wavelengths for MnPc. A new peak at 317 nm was observed corresponding to a charge transition from Pc to Phenyl rings (ligands) (CT3).

Fig. 7 shows the electrostatic potentials and total electron densities of the investigated systems in DMF. For Ni and Co Pcs, the core is negatively charged and the positive charges are distributed on the exterior parts of the ligands. On the other hand, MnPc shows a different charge distribution as the whole systems seems to equally share the charges having a neutral character except a negative small region on the exterior parts of the ligands. Since ESP indicates negative and positive regions of a molecule, it can be said that **4** will have the lowest conductivity among others.

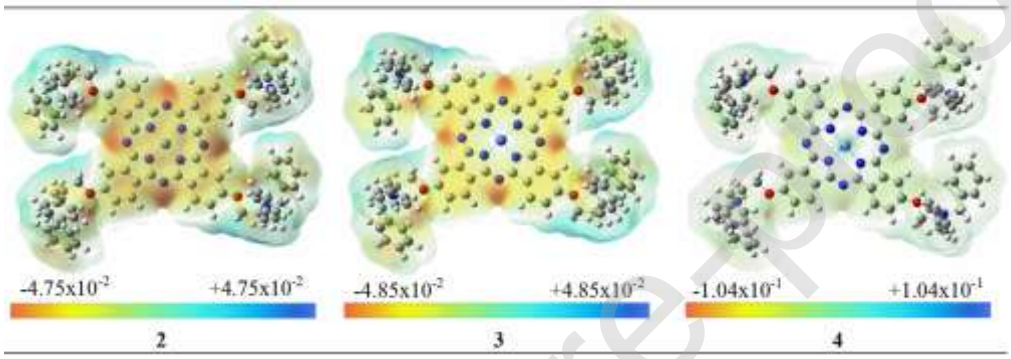

Fig. 7. Total electron densities with electrostatic potentials (a.u.) calculated with B3LYP/6-31G(d,p) and LANL2DZ (on metals) (Color coding: red, electron rich; yellow, slightly electron rich region; green, neutral; light blue, slightly electron deficient; blue, electron deficient)

3.3. DC Conductivity properties

Current-voltage (*I*-*V*) characteristics were determined between the temperatures 293-523 K to obtain dc conductivity properties of the compounds. DC conductivity (σ_{dc}) values of the films were calculated using the slope of *I*–*V* plots and the equation $\sigma_{dc}=(I/V)(d/(2n\text{-}1)lh)$ where, (I/V) is slope of the *I*–*V* plot, *d* is separation between the gold electrodes, *n* is number of the finger pairs, *l* is overlap length and *h* is thickness of the electrodes. Electrical measurements were done in home-made aluminum chamber

in vacuum (2×10^{-3} mbar) in dark. Fig. 8 shows dc conductivity values of the films **2 - 4** as a function of temperature. Dashed lines represent fitting lines for the films for two different temperature regions, $T< 478$ K, and $T\geq 478$ K. Slope of the fitting lines for the temperature range of $T< 478$ K were found as -7.61, -6.13, and -7.95 for **2**, **3** and **4** respectively. From regression analysis, R^2 values were found as 0.992, 0.994 and 0.993 for **2**, **3** and **4** respectively. As plotted in the figure, conductivity of the films, sensitive to temperature, showed nearly linear behavior with increasing temperature indicating semiconducting behavior. DC conductivities were calculated as $5.29\text{x}10^{-10}$ S/cm, $2.39\text{x}10^{-9}$ S/cm, $3.04\text{x}10^{-10}$ S/cm, and for the films **2**, **3** and **4** at room temperature, respectively. Compound **3** showed higher conductivity among the others and the conductivity values can be ordered as $\sigma_{(4)}<\sigma_{(2)}<\sigma_{(3)}$. The values were increased with increasing temperature and reached to the values of $1.34\text{x}10^{-5}$ S/cm, $1.26\text{x}10^{-5}$ S/cm, and $1.30\text{x}10^{-5}$ S/cm, for the films of **2**, **3** and **4** respectively, at 523 K. Slope of the **3** was constant until 478 K then the rate of the slope showed small decrease with temperature. DC conductivity values of the films **2-4** were found in the range of the previous reports [23,24].

The linear variation of ln σ_{dc} with temperature, presented in Fig. 8, can be expressed by well known Arrhenius equation (Eq. 1),

$$\sigma_{dc} = \sigma_o e^{-(E_A/k_B T)} \quad (1)$$

where σ_o is coefficient of exponential function that gives the specific conductivity for the conduction as $T\rightarrow\infty$, E_A is activation energy, k_B is Boltzmann's constant, and T is temperature. Table 1 presents calculated activation energy values of **2-4** with aid of Arrhenius plots, presented in Fig. 8. The values in Table 1 are in agreement with the values reported earlier [23–25].

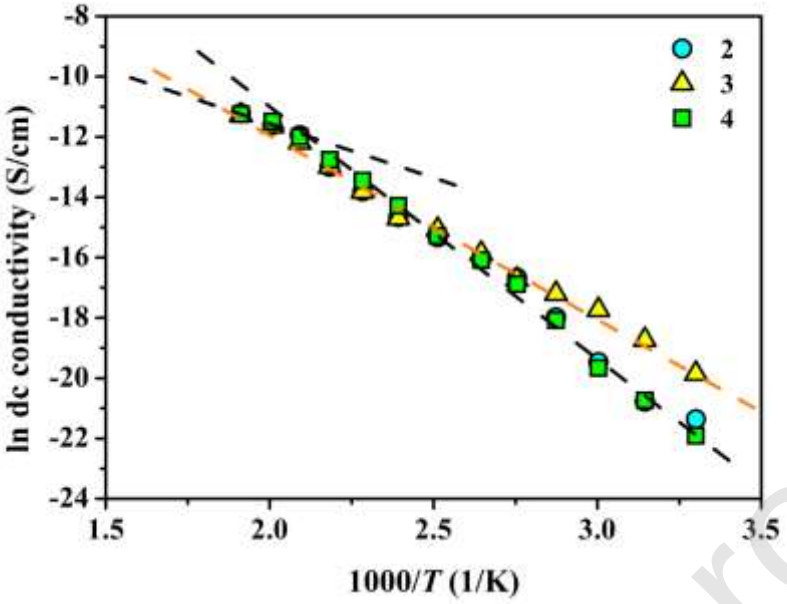

Fig. 8. DC Conductivity values of the **2-4** versus temperature.

Table 1. Activation energy values for the films **2-4** (E_{A1} for T< 478 K, E_{A2} for T≥ 478 K).

Film	E_{A1} **(eV)**	E_{A2} **(eV)**
2	0.67	0.35
3	0.50	0.26
4	0.70	0.36

3.4. AC Conductivity properties

To determine ac conductivity properties and charge transport mechanism in the compounds under investigation, ac conductivity measurements were done on the **2-4** with respect to frequency (40 Hz-100 kHz) in the temperature range of 293-523 K in vacuum (2×10^{-3} mbar) in dark. In Fig. 9, ac conductivity values of **4** were plotted with respect to frequency for some temperatures. By inspecting the Fig. 9**,** ac conductivity of the film **4** increased with increasing temperature and frequency. Another

observation on the Fig. 2 that rate of increase of conductivity changed at different temperature and frequency regions. Frequency dependence of the ac conductivity for $T \leq$ 418 K are greater than that of $T >$ 418 K. The variation of conductivity with temperature and frequency shown in Fig. 9 were similar to that of **2** and **3**.

Behavior of the ac conductivity of **2 – 4** with frequency can be represented by Eq. 2.

$$\sigma_{ac} = A\omega^{s} \quad (2)$$

where A and s are constants and ω is the angular frequency. *S* values in Eq. 2 were calculated for **4** from slopes of the ac conductivity versus frequency curves presented in Fig. 9 for three different frequency regions (f < 1 kHz, 1 Hz ≤ f ≤ 10 kHz and f ≥ 10 kHz).

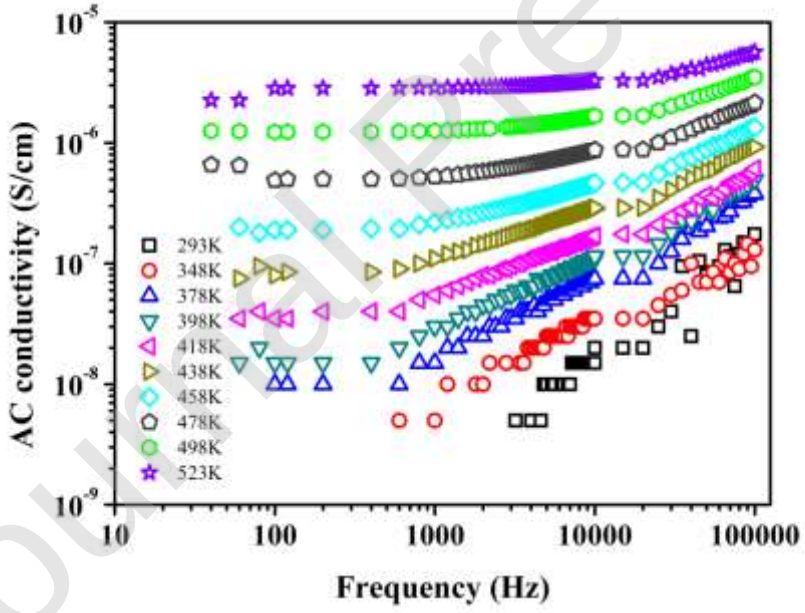

Fig. 9. AC Conductivity values of the **4** versus frequency at indicated temperatures.

Fig. 10A presents *s* values vs. temperature plots of **4** for three different frequency regions, and reveals that s values decreased with increasing temperature. Because of

the limits of the LCZ meter, *s* values at frequencies $f < 10^3$ Hz and at the temperatures $T < 348$ K were not presented. The curves for s values for the **2** and **3** were similar to that of **4** with $s < 1$. For comparison, Fig. 10B presents *s* values vs. temperature plots of **2-4** in the frequency region 1 kHz $\leq f \leq$ 10 kHz.

According to band theory, ac conductivity behavior should not depend on frequency and drops at high frequency. According to the quantum mechanical tunneling (QMT) model [26], *s* values in Eq. 2 equal to 0.8 and either increase as a function of temperature or does not depend of temperature. Therefore this model is not applicable to our results. In overlapping-large polaron tunnelling (QLPT) model [27], *s* values in Eq. 2 depend on frequency and temperature and decrease with respect to temperature to a lowest value at some temperature then the values increase with respect to temperature. So this model can not be applicable to our results. In small polaron quantum mechanical tunnelling (SP) model, *s* values in Eq. 2 increase with increasing temperature [28].

In hopping model, ac conductivity increases with increasing frequency ($s \leq 1$). In this model, charge transports are performed by mobile carriers and the carriers hop between sites. There are potential barriers between the sites [28]. In Correlated Barrier Hopping (CBH) model [27,28] *s* values in Eq. 2 decrease with increasing temperature and given by Eq. 3.

$$s = 1 - \beta = 1 - \frac{6 k_B T}{W_m} \tag{3}$$

where k_B is Boltzmann's constant and W_m is the binding energy and T is temperature in Kelvin. Low *s* values indicate a multihopping process, while high s values indicate a single hopping process. Based on these models, the present investigation leads to the following inferences.

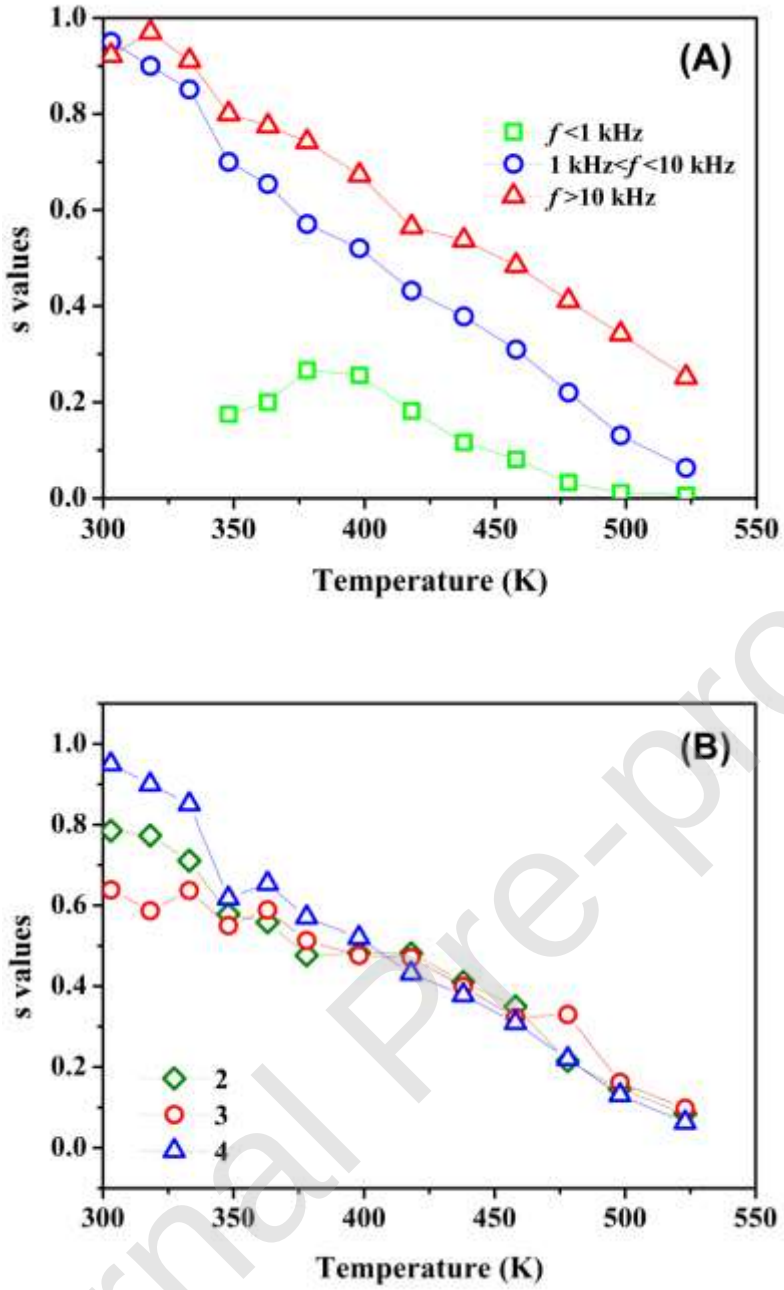

Fig. 10. Variation of *s* values with temperature (a) for **4** at indicated frequency regions (b) for **2- 4** for *f*≥ 10 kHz.

Our findings revealed that behavior of *s* values with respect to temperature and behavior of σ_{ac} with respect to frequency are consistent with the hopping model. AC charge transport mechanism for **2-4** can be analyzed in terms of temperature and

frequency. Same type of temperature dependence for *s* values reported earlier for different phthalocyanine films [24,29,30].

At $T \geq 438$ K, dominant conduction mechanism can be represented by single hopping. At $T < 438$ K, conduction mechanism can be interpreted with frequency region. Dominant conduction mechanism can be represented by multihopping in the frequency range $f < 1$ kHz and by single hopping for $f \geq 1$ kHz for the studied films.

3.5. CO_2 Sensing properties

Effects of relative humidity (RH) on carbon dioxide sensing properties of the films of **2-4** were investigated as a function of gas concentration (1000-8000 ppm) at room temperature (293 K) in air. Additionally, in order to investigate effect of the relative humidity on sensing properties, the measurements were also performed in a wide range of relative humidity, 0-80% RH. CO_2 sensing measurements were performed after the current passing through the sensor in air/humid air atmosphere remains constant (steady-state). Gas sensing properties were obtained for 300 seconds intervals; 300 seconds for CO_2 and 300 seconds for purging with air (0-80% RH), consecutively. In order to measure the current passing through the sensors 1 V (dc) was applied to the electrodes of the sensors.

Fig. 11 presents variation of normalized sensor current with time (dynamic sensing characteristic) of the sensor **3** for different concentrations of CO_2 at 293 K and in different humid air (20 – 80% RH) ambient. Normalized current is defined as I_{gas}/I_{air}, where I_{gas} and I_{air} are the current passing through the sensor under CO_2 exposure and in humid air, respectively. Since normalized current (current normalized to 1, $I_{air}/I_{air}=1$ at initial (0 – 300 sec)) plotted as a function of time, there is no unit for normalized current presented in vertical axes. Response of the sensor **3** for RH less than 20% is not

presented because of small response towards CO_2. The CO_2 concentrations were 1000, 2000, 4000, 6000 and 8000 ppm.

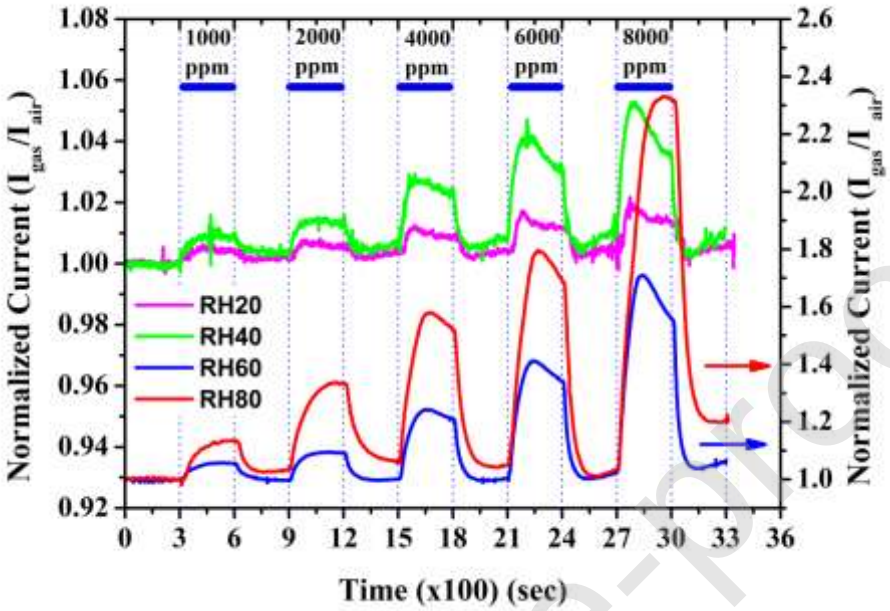

Fig. 11. Variation of normalized sensor current with time of the **3** towards different CO_2 concentrations (1000, 2000, 4000, 6000 and 8000 ppm) in humid air (20-80% RH) at 293 K (20 and 40% RH use left axis, 60 and 80% RH use right axis) $(V(dc)_{applied}=1\ V)$.

Dynamic sensing characteristics of the sensor **3** in humid air can be examined as a function of *i)* CO_2 concentration and *ii)* relative humidity (RH). When response of the sensor **3** examined as a function of CO_2 concentration, as seen in Fig. 11, sensor **3** showed good response towards CO_2 and current passing through the sensor increased sharply after the sensor exposed to CO_2 and in five minutes of exposure to CO_2, the current of the sensor **3** reached to saturation. Adsorption processes is reversible since current of the sensor **3** decreased almost to its initial value in five minutes recovery interval, for each recovery process. It was also observed that change in current increased with increasing CO_2 concentration at each humidity level tested. Since there

is small response towards CO_2 between the RH percentages of 0-%20 RH, effect of humidity on CO_2 sensing properties were presented in humid air for 20-80% RH. Sensor **3** behaves like a p-type semiconductor because of current passing through the **3** increases in presence of oxidizing gas, CO_2 [31,32]. Our results showed that $((I_{gas}-I_{air})/I_{air}) > 1$) and this result is consistent with previous reports for p-type semiconductors [31]. When response of the sensor **3** towards CO_2 examined as a function of relative humidity, it is easily to see that CO_2 response of the sensor **3** is strongly affected by percentage of the RH and the change in current passing through the sensor in the presence of CO_2 increased with increasing RH. As relative humidity approaches from 20% to 80% normalized current passing through the sensor **3** increased from $1.6x10^{-2}$ to 1.3 for 8000 ppm CO_2. Similar increasing response towards CO_2 with increasing RH percentage has been reported earlier [31,33]. The effects of CO_2 on the sensor **3** in humid air (for all % RH ambient) are significantly greater in magnitude, compared to those in dry air (0% RH). Additionally, the quality of the sensor signals in humid air with 80% RH is better than that of in humid air with RH < 80% as in Fig. 11. Similar increasing quality signal of the sensor with increasing relative humidity was observed between dry air and humid air ambient. Greater response of the sensor towards CO_2 in humid air, especially for relative humidity conditions greater than 40% RH, indicates applicability of the sensor for real operating conditions.

CO_2 sensing mechanism regarding to interaction between sensing materials and CO_2 can be explained as follows: Sensing behavior of the Pc based sensors depends on change in conductivity due to interaction between surface of sensing material and test gas (physisorption). When sensing film exposed to CO_2, sensing film donate electrons to CO_2 gas. That increases the conductivity of p-type materials and results an increase

in current passing through the sensor. The current passing through the sensor increases upon exposure to CO_2, with p-type behavior, according to the following Eq. (4):

$$CO_2 + e^- \Leftrightarrow CO_2^- \quad (4)$$

It was also observed that humidity caused to increase the current passing through the sensor. Same behavior was also reported by different authors. According to author's reports, current increases because of the dissociation of proton ($H^{\pm}$) or hydronium ion ($H_3O^{\pm}$) from H_2O molecules. As a result of this dissociation, proton ($H^{\pm}$) or $H_3O^{\pm}$ can move more freely on the water layer which is condensed on the sensing film producing an increase in current passing through the sensor [10,34,35]. This mechanism at high relative humidity (RH) ambient is known as Grotthuss mechanism. As mentioned above, as humidity levels increase, the protons (H^+) can move more easily and correspondingly caused to an increase in current passing through the sensing film.

When sensor exposed to CO_2 in the presence of humidity, CO_2 reacts with H_2O to form carbonic acid (H_2CO_3). Carbonic acid then dissociates H^+ (protons) and HCO_3^- (hydrogen carbonate ions). These ions may come in contact with the sensing material and results an increase in current passing through the sensor. Increased levels of CO_2 lead to more carbonic acid forming therefore more H^+ and HCO_3. The change in current of the sensors should be dependent on the concentration of hydrogen carbonate ions corresponding to concentration of CO_2 and H_2O. Similar interpretations for CO_2 sensors working in humid ambient, using base-type poly(anthranilic acid) (PANA) and poly(vinyl alcohol) (PVA) sensing material, were reported earlier [35].

According to the interpretations, it could be said that, an increase in relative humidity percentages may enhances response of the sensors towards CO_2.

In order to compare the dynamic sensing characteristics of the sensors **2-4**, Fig. 12 is presented. The figure shows variation of the normalized current passing through the

sensors **2-4** towards CO_2 (1000, 2000, 4000, 6000, and 8000 ppm) for 60% RH at 293 K. By examining Fig. 12, effect of the metal atoms **2-4** in the compounds on sensing properties can be seen clearly.

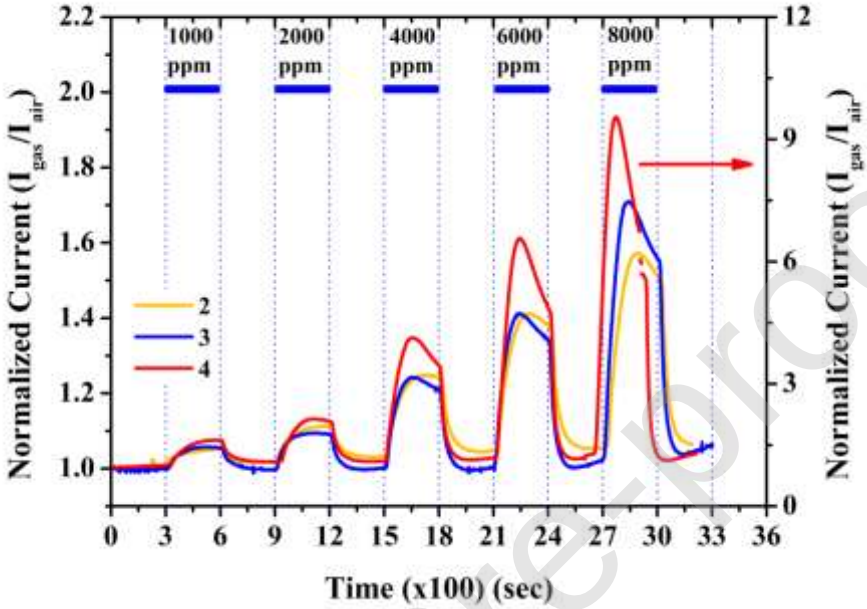

Fig. 12. Variation of normalized sensor current with time of **2-4** towards CO_2 for 60% RH at 293 K (**4** uses right axis and **2**, **3** use left axis). $(V(dc)_{applied}=1\ V)$.

CO_2 sensitivity of the sensors can be defined as [36,37] similarly,

$$S = \left(\frac{I_{gas} - I_{air}}{I_{air}} \right) \quad (5)$$

where I_{gas} and I_{air} are the current passing through the sensor under CO_2 exposure and in humid air, respectively. Sensitivity of the sensors plotted as a function of CO_2 concentration at different RH percentages at 293 K. Sensitivity of the sensor **3** is presented in Fig. 13A for 20, 40, 60, and 80% RH. The lines in the figure were drawn for eye guidance. As seen from the Fig. 13A that, sensitivity of **3** increases with increasing CO_2 concentration and relative humidity. As explained above sensitivity of

the **3** enhanced by higher humidity levels indicating applicability of the sensor in daily life conditions.

In order to compare the sensitivity of the sensors **2-4** with increasing CO_2 concentration and humidity at room temperature, Fig. 13b is presented. In this figure, as a representative result, comparison of the sensitivity of the sensors **2-4** as a function of CO_2 concentration presented for relative humidity levels at 60% RH and 80% RH. It can be seen clearly, the sensors **2-4** showed good sensitivity towards CO_2 and sensitivity of the sensors increased with increasing CO_2 concentration and humidity. While sensitivity of the sensor **2** at 80% RH for 1000 and 8000 ppm were 0.076 and 0.557, the values were calculated as 0.135 and 1.296 for **3** and 0.790 and 3.002 for **4**. Sensitivity (S) of the sensors can be ordered as $S_{(4)} > S_{(3)} > S_{(2)}$. From the Fig. 13B, it can be concluded that best sensitivity values were observed for the sensor **4**. From regression analysis, R^2 values were found greater than 0.94 except **4** (RH 80%) and the values were presented in Fig. 13A, and 13B.

The solubility of the manganese phthalocyanine complex is higher than that of other metal complexes (NiPc and CoPc) which is attributable to the central metal ion with less charge density. The fact that the aggregation of this manganese complex is lower than the others, increases the binding possibility of acidic CO_2 to dibenzylamino nitrogen at the peripheral structure. Therefore, the interaction between MnPc (**4**) and CO_2 may result in higher sensitivity than the other two metallophthalocyanines (NiPc (**2**) and CoPc (**3**)).

A former study on MnPc (**4**) has revealed that it is limited to CO_2 sensing due to the weak van der Waals interactions between CO_2 and Mn center [38]. Our results indicate that humidity increases the sensitivity of **4** for CO_2 in addition to the explanations given above.

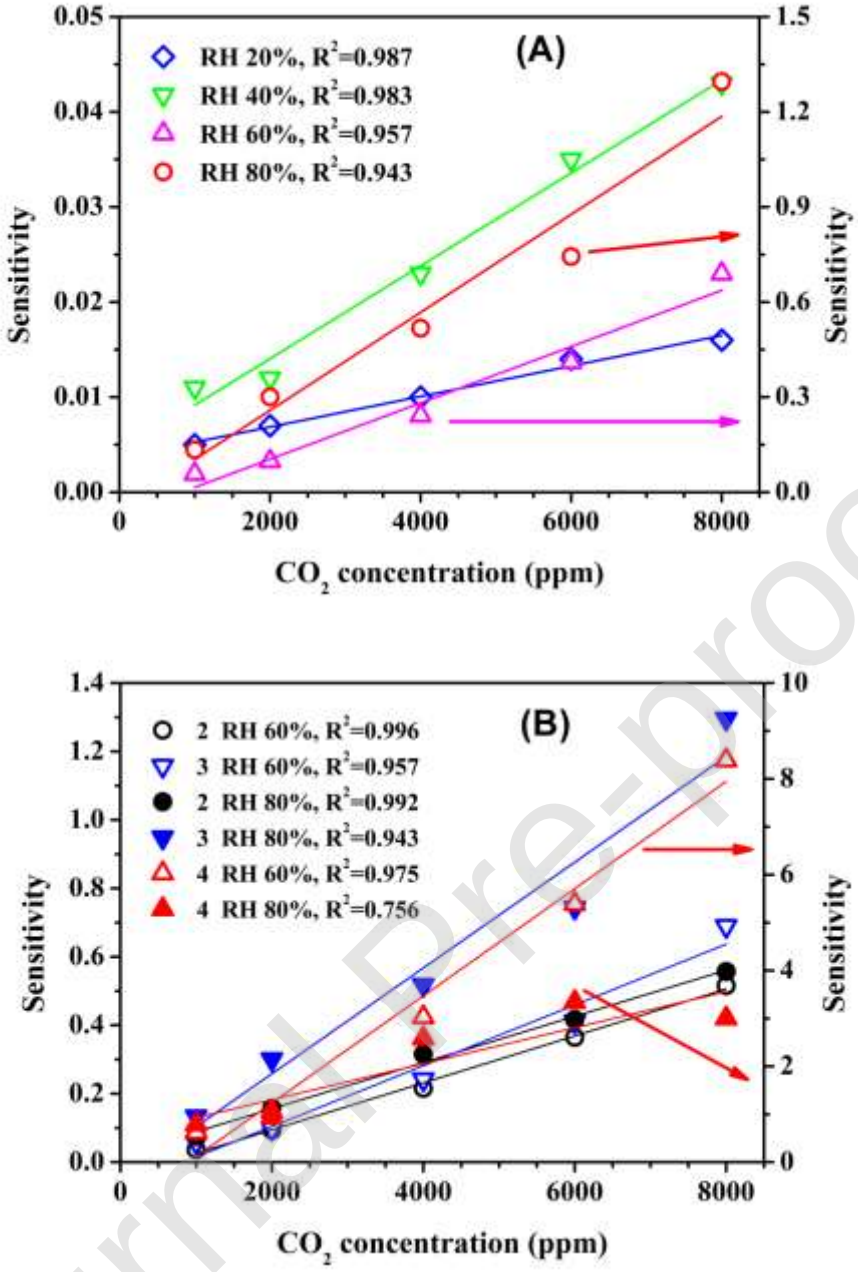

Fig. 13. Sensitivity curves as a function of CO_2 concentration at 293 K (a) for **3** at indicated RH ambient (b) for **2-4** at 60% RH and 80% RH (**4** use right axis, and rest of the sensors use left axis).

Response time values (τ_{90}) were defined as a time interval between the time of exposure and the time 90% of total change in current in the measurement time interval

at indicated concentration and relative humidity (RH). Longer response time (τ_{90}) means slow response of the sensors towards CO_2. Under humid conditions, the response time and recovery times are found much shorter than the exposure time.

Fig. 14a shows response time values of the **3** depending on CO_2 concentration at different relative humidity ambient. The lines in the figure were drawn for eye guidance. Response time values, in general, tend to decrease with increasing CO_2 concentration. However, the values were increased with increasing relative humidity percentages. Response time values took placed between 60-73 seconds at 20% RH. The values increased to 118-168 seconds at higher humid level, 80% RH. In order to compare the response time values of the sensors **2-4** with increasing CO_2 concentration and humidity, Fig. 14b is presented. In this figure, as a representative result, comparison of the response time values of the sensors **2-4** as a function of CO_2 concentration presented for relative humidity levels at 60% RH and 80% RH. Response time values for **3** were found shorter than the other sensors at 60% and 80% RH but longer response time values were obtained for **2** than the other sensors at 60% RH and for **4** at 80% RH. Another remarkable observation is that while response time values tend to decrease with increasing CO_2 concentration for 60% RH, the values decreased until 4000 ppm CO_2 then increased for 80% RH. In general response time values took placed between 39-200 seconds depending on CO_2 concentration and relative humidity level.

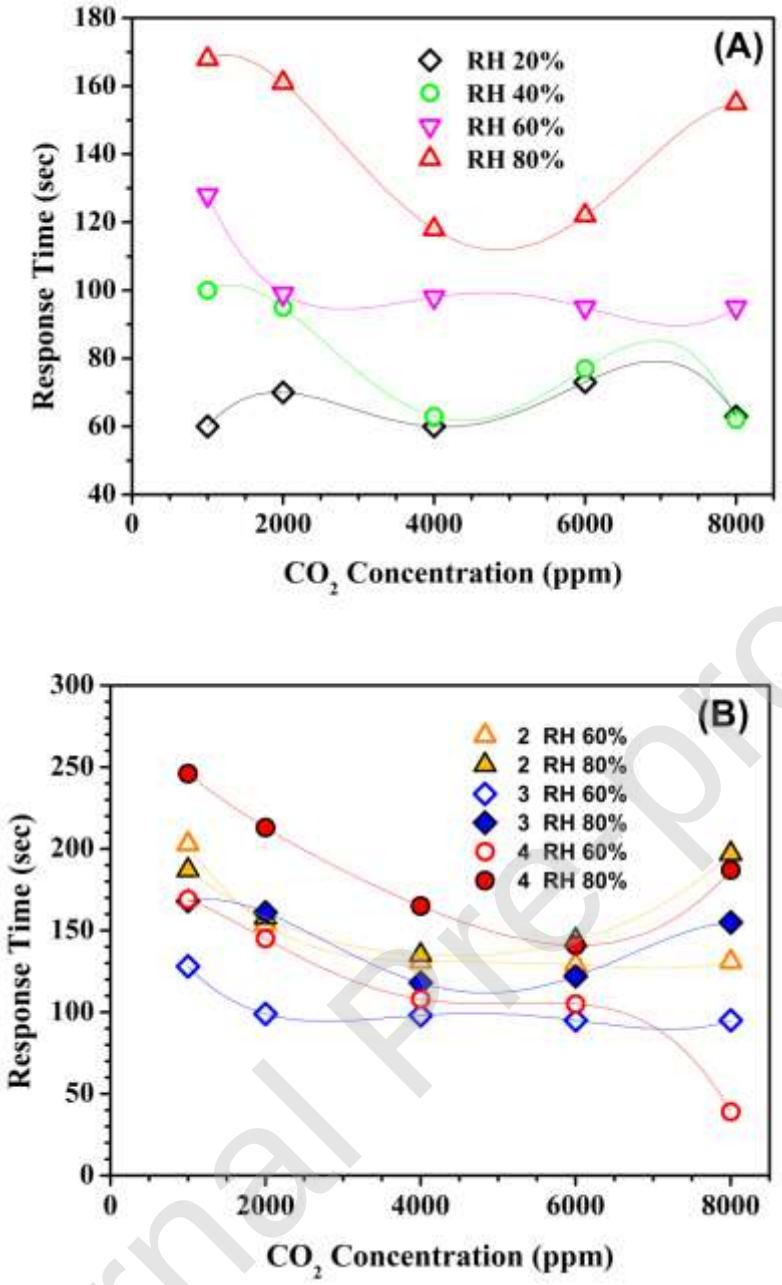

Fig. 14. Response time values towards CO_2 at indicated % RH percentages at 293 K **(a)** for **3** **(b)** for **2-4** at 60% RH and 80% RH.

4. Conclusions

Novel tetrakis-[dibenzyl amino ethoxyl] substituted Pc complexes with Ni(II), Co(II) and Mn(II) metal ions were achieved and characterized using IR, ^{1}H-NMR, ^{1}H-^{1}H-COSY-NMR, UV-vis and MALDI TOF MS spectroscopic methods. The UV-vis

absorption spectra of the molecules obtained by DFT calculations were found in agreement with the experimental spectra and were used to determine the characteristics of the electronic transitions for the compounds. DC conductivity measurements showed that $\sigma_{(4)}<\sigma_{(2)}<\sigma_{(3)}$ at room temperature in vacuum in dark. An increase in temperature caused increase in dc conductivity of the films of the compounds indicating semiconducting property. Activation energies of the **2-4** varied between 0.5-0.7 eV at the temperature region $T<$ 478 K. AC conductivity results suggest that dominant charge transport mechanisms can be modeled by single hopping and multi-hopping model depending on temperature and frequency range. Dynamic response of the sensors revealed that response of the sensors reversible and sensitivities increase with increasing CO_2 concentration and relative humidity. Sensor **4** showed best sensitivity towards CO_2. Higher relative humidity values enhanced the sensitivity of the sensors towards CO_2.

Conflicts of interest

There are no conflicts to declare.

Acknowledgements

This work was supported by Ministry of Development-Republic of Turkey with the project Number: 2016 K121230. Özer Bekaroğlu and Bekir Salih gratefully acknowledge the Turkish Academy of Science (TUBA) for the partial financial support. Authors also thank to Marmara University Scientific Research Committee (Project Numbers: FEN-C-YLP-120917-0552, FEN-D-120418-0176 and FEN-BGS-290506-0114) for their support. The authors are grateful to the TUBITAK-ULAKBIM Truba Resources for computer time.

Appendix A. Supplementary data

Computational results including ligand conformers, electronic transitions and corresponding molecular orbitals for investigated systems are given in Supplementary Information.

References

[1] Ö. Bekaroğlu, Phthalocyanines containing macrocycles, Appl. Organomet. Chem. (1996). doi:10.1002/(SICI)1099-0739(199610)10:8<605::AID-AOC527>3.0.CO;2-U.

[2] P.A. Stuzhin, Azaporphyrins and Phthalocyanines as Multicentre Conjugated Ampholites, J. Porphyr. Phthalocyanines. (1999).

[3] M. Hanack, M. Lang, Conducting Stacked Metallophthalocyanines and Related Compounds, Adv. Mater. (1994). doi:10.1002/adma.19940061103.

[4] A.B. Sorokin, Phthalocyanine metal complexes in catalysis, Chem. Rev. (2013) 8152–8191. doi:10.1021/cr4000072.

[5] Occupational Health Guideline for Carbon Dioxide, (n.d.). https://www.cdc.gov/niosh/docs/81-123/pdfs/0103.pdf?id=10.26616/NIOSHPUB81123.

[6] D. Hunter, The Diseases of Occupations, 5th ed., Hazell Watson and Viney Ltd., Aylesburg, 1975.

[7] CO2, (n.d.). https://www.cdc.gov/niosh/idlh/124389.html.

[8] D. Wang, Y. Chen, Z. Liu, L. Li, C. Shi, H. Qin, J. Hu, CO2-sensing properties and mechanism of nano-SnO2 thick-film sensor, Sensors Actuators, B Chem. 227 (2016) 73–84. doi:10.1016/j.snb.2015.12.025.

[9] M. Sülü, A. Altindal, Ö. Bekaroğlu, Synthesis, characterization and electrical and CO2 sensing properties of triazine containing three dendritic phthalocyanine, Synth. Met.

155 (2005) 211–221. doi:10.1016/j.synthmet.2005.08.005.

[10] X. Wang, Y. Chen, H. Qin, L. Li, C. Shi, L. Liu, J. Hu, CO2 sensing of La0.875Ca0.125FeO3 in wet vapor: A comparison of experimental results and first-principles calculations, Phys. Chem. Chem. Phys. 17 (2015) 13733–13742. doi:10.1039/c5cp00096c.

[11] N.B. Borchert, J.P. Kerry, D.B. Papkovsky, A CO2 sensor based on Pt-porphyrin dye and FRET scheme for food packaging applications, Sensors Actuators, B Chem. 176 (2013) 157–165. doi:10.1016/j.snb.2012.09.043.

[12] S. Xu, C. Li, H. Li, M. Li, C. Qu, B. Yang, Carbon dioxide sensors based on a surface acoustic wave device with a graphene-nickel-l-alanine multilayer film, J. Mater. Chem. C. 3 (2015) 3882–3890. doi:10.1039/c4tc02986k.

[13] D.J.F. M.J. Frisch, G.W. Trucks, H.B. Schlegel, G.E. Scuseria, M.A. Robb, J.R. Cheeseman, G. Scalmani, V. Barone, B. Mennucci, G.A. Petersson, H. Nakatsuji, M. Caricato, X. Li, H.P. Hratchian, A.F. Izmaylov, J. Bloino, G. Zheng, J.L. Sonnenberg, M. Hada, M. Ehar, Gaussian 09 C.01, Gaussian, Inc. Wallingford CT. (2010).

[14] R. Dennington, T. Keith, J. Millam, GaussView, Version 5., Semichem Inc. , Shawnee Mission. KS. (2009).

[15] W. Kohn, L.J. Sham, Self-consistent equations including exchange and correlation effects, Phys. Rev. 140 (1965) A1133–A1138. doi:10.1103/PhysRev.140.A1133.

[16] A. D. Becke, Density-functional exchange-energy approximation with correct asymptotic behavior, Phys. Rev. A. 38 (1988) 3098–3100. doi:10.1103/PhysRevA.38.3098.

[17] A.D. Becke, Density-functional thermochemistry. III. The role of exact exchange, J. Chem. Phys. 98 (1993) 5648–5652. doi:10.1063/1.464913.

[18] C. Lee, W. Yang, R.G. Parr, Development of the Colle-Salvetti correlation-energy

formula into a functional of the electron density, Phys. Rev. B. 37 (1988) 785–789. doi:10.1103/PhysRevB.37.785.

[19] J. and P.J.H. T. H. Dunning, Gaussian Basis Sets for Molecular Calculations, in: H.F. Schaefer (Ed.), Mod. Theor. Chem., Plenum Publishing Company, New York, 1977: pp. 1–28.

[20] J. Tomasi, B. Mennucci, E. Cancès, The IEF version of the PCM solvation method: An overview of a new method addressed to study molecular solutes at the QM ab initio level, in: J. Mol. Struct. THEOCHEM, 1999: pp. 211–226. doi:10.1016/S0166-1280(98)00553-3.

[21] J. Tomasi, B. Mennucci, R. Cammi, Quantum mechanical continuum solvation models, Chem. Rev. (2005) 2999–2094. doi:10.1021/cr9904009.

[22] Spartan 08 for Windows, (n.d.).

[23] E. Ermiş, Y. Çimen, F. Dumludağ, A.R. Özkaya, B. Salih, Ö. Bekaroğlu, Electrochemical and electrical properties of novel mono and ball-type phthalocyanines, Polyhedron. (2013). doi:10.1016/j.poly.2012.09.048.

[24] B. Köksoy, M. Aygün, A. Çapkin, F. Dumludağ, M. Bulut, Electrical and gas sensing properties of novel cobalt(II), copper(II), manganese(III) phthalocyanines carrying ethyl 7-oxy-4,8-dimethylcoumarin-3-propanoate moieties, J. Porphyr. Phthalocyanines. (2018). doi:10.1142/S1088424618500153.

[25] Y. Çimen, E. Ermiş, F. Dumludağ, A.R. Özkaya, B. Salih, Ö. Bekaroğlu, Synthesis, characterization, electrochemistry and VOC sensing properties of novel ball-type dinuclear metallophthalocyanines, Sensors Actuators, B Chem. (2014). doi:10.1016/j.snb.2014.06.066.

[26] A. Ghosh, Frequency-dependent conductivity in bismuth-vanadate glassy semiconductors, Phys. Rev. B. (1990). doi:10.1103/PhysRevB.41.1479.

[27] A.R. Long, Frequency-dependent loss in amorphous semiconductors, Adv. Phys. 31 (1982) 553–637. doi:10.1080/00018738200101418.

[28] S.R. Elliott, A.c. conduction in amorphous chalcogenide and pnictide semiconductors, Adv. Phys. 36 (1987) 135–218. doi:10.1080/00018738700101971.

[29] E. Yabaş, M. Sülü, S. Saydam, F. Dumludağ, B. Salih, Ö. Bekaroğlu, Synthesis, characterization and investigation of electrical and electrochemical properties of imidazole substituted phthalocyanines, Inorganica Chim. Acta. 365 (2011) 340–348. doi:10.1016/j.ica.2010.09.054.

[30] T. Ceyhan, A. Altindal, M.K. Erbil, Ö. Bekaroğlu, Synthesis, characterization, conduction and gas sensing properties of novel multinuclear metallo phthalocyanines (Zn, Co) with alkylthio substituents, Polyhedron. (2006). doi:10.1016/j.poly.2005.07.046.

[31] A. Marsal, G. Dezanneau, A. Cornet, J.R. Morante, A new CO2 gas sensing material, in: Sensors Actuators, B Chem., 2003: pp. 266–270. doi:10.1016/S0925-4005(03)00443-X.

[32] A. Marsal, A. Cornet, J.R. Morante, Study of the CO and humidity interference in La doped tin oxide CO2 gas sensor, Sensors Actuators, B Chem. 94 (2003) 324–329. doi:10.1016/S0925-4005(03)00461-1.

[33] I. Djerdj, A. Haensch, D. Koziej, S. Pokhrel, N. Barsan, U. Weimar, M. Niederberger, Neodymium dioxide carbonate as a sensing layer for chemoresistive CO 2 sensing, Chem. Mater. 21 (2009) 5375–5381. doi:10.1021/cm9013392.

[34] Y. Tan, K. Yu, T. Yang, Q. Zhang, W. Cong, H. Yin, Z. Zhang, Y. Chen, Z. Zhu, The combinations of hollow MoS2micro@nano-spheres: One-step synthesis, excellent photocatalytic and humidity sensing properties, J. Mater. Chem. C. 2 (2014) 5422–5430. doi:10.1039/c4tc00423j.

[35] Z. Wang, Y. Xiao, X. Cui, P. Cheng, B. Wang, Y. Gao, X. Li, T. Yang, T. Zhang, G. Lu, Humidity-sensing properties of urchinlike CuO nanostructures modified by reduced graphene oxide, ACS Appl. Mater. Interfaces. 6 (2014) 3888–3895. doi:10.1021/am404858z.

[36] K.R. Nemade, S.A. Waghuley, Optical and Gas Sensing Properties of Cuo Nanoparticles Grown by Spray Pyrolysis of Cupric Nitrate Solution, Int. J. Mater. Sci. Eng. 2 (2014) 63–66. doi:10.12720/ijmse.2.1.63-66.

[37] R. Kumar, J. Mittal, N. Kushwaha, B. V. Rao, S. Pandey, C.P. Liu, Room temperature carbon monoxide gas sensor using Cu doped OMS-2 nanofibers, Sensors Actuators, B Chem. 266 (2018) 751–760. doi:10.1016/j.snb.2018.03.182.

[38] D. Zou, W. Zhao, B. Cui, D. Li, D. Liu, Adsorption of gas molecules on a manganese phthalocyanine molecular device and its possibility as a gas sensor, Phys. Chem. Chem. Phys. 20 (2018) 2048–2056. doi:10.1039/c7cp06760g.

Biographies

Sema Şenoğlu obtained her B.Sc. degree in Chemistry in 2016 from Marmara University, Istanbul, Turkey. She completed her M.Sc. degree in the year 2019 from the same University. Her research interest is mainly in synthesis and analytical investigation of metallo phthalocyanines.

Metin Özer obtained his B.Sc. in Chemical Engineering in 1989 from Istanbul University and the Master and Doctoral degree in Chemistry from Marmara University, İstanbul, Turkey. He is full professor since 2017 at the same department. His research interests are focused on synthesis, electrochemical and gas sensor applications of metallo phthalocyanines.

Fatih Dumludağ received his PhD in physics from Marmara University in 2000. He has worked as visiting researcher in Centre for Molecular Electronics, School of Engineering,

Durham University, U.K. He is presently working as associate professor in Department of Physics, Marmara University, Istanbul, Turkey. His current research interest involves chemical sensors, biosensors, solar cells and OFETs with nanocrystals and nanowires.

Nursel Acar received her MSc and PhD in chemistry from Ege University in 1994 and 2000, Izmir, Turkey. She was scholar from DAAD in Institute of Physical and Electrochemistry, TU University Dresden, Germany in 1998. She worked as a post-doctoral research fellow between 2001 and 2003 in Physical Chemistry at FAU Erlangen, Germany. She worked on electron transfer systems in natural and artificial photosynthetic systems and effect of structure and geometry on sensor photoreceptors. She is presently working as associate professor in Department of Chemistry, Ege University, Izmir, Turkey. Her research interests are in the areas of physical chemistry, photochemistry and computational chemistry.

Bekir Salih received his BS and MSc degrees in chemistry from Hacettepe University in 1981 and 1983. He got PhD from Hacettepe University with first degree in mass spectrometry. He became Assistant Professor in 1992, Associated Professor in 1997 and Full Professor in 2001 at Hacettepe University. In 1998–1999, he spent more than 1 year in ETH-Zurich-Switzerland as a visiting professor and worked on new mass spectrometric techniques such as MALDI-MS, ESI-MS and FT-ICR-MS with Prof. Dr. Renato Zenobi. He is the instrumental analysis expert of International Atomic Energy Agency from 2001 in the area of the south part of the world. He has been working mainly on new mass spectrometric techniques. His main research area is covered proteomics, drugtomics, new MALDI target surfaces without matrix used, sol–gels, and enzyme immobilization for proteomics applications, polymer analysis and mechanistic work on MALDI matrices.

Özer Bekaroğlu received BS and MS in chemical engineering from University of İstanbul 1960, PhD from University of Basel (Switzerland) 1963 in the field of coordination chemistry. After posdoctoral work at the University of California, Davis 1966–1968, worked

at a pharmaceutical company as Investment Manager for 1 year. He became Associated Professor at the University of İstanbul in 1969. Upon invitation, transferred to the Technical University of İstanbul and became full professor in 1975. He was invited as Guest Professor by several universities in Europe and Japan from three to eight months. He was Dean at the several faculties for 9 years. He also was Head of Department of Chemistry of the Turkish Scientific and Industrial Research Council for 10 years, and head of department of inorganic chemistry of Technical University of Istanbul until his retirement in 2000. He still contiues his research studies in Istinye University, Istanbul, Turkey. His research is mainly focused on syntheses and properties of new class of phthalocyanines since 1985. He published over 200 papers in SCI journals. He is honorary member of "Turkish Academy of Sciences".

Table 1. Activation energy values for the films **2-4** (E_{A1} for T< 478 K, E_{A2} for T≥ 478 K).

Film	E_{A1} **(eV)**	E_{A2} **(eV)**
2	0.67	0.35
3	0.50	0.26
4	0.70	0.36